ORIGINAL PAPER

One-step fabrication in aqueous solution of a granular alginate-based hydrogel for fast and efficient removal of heavy metal ions

Wenbo Wang · Yuru Kang · Aiqin Wang

Abstract Granular alginate-based hydrogels were prepared in situ in an aqueous solution via grafting and crosslinking reactions among sodium alginate (SA), acrylic acid (AA), polyvinylpyrrolidone (PVP), and gelatin (GE). Fourier transform infrared spectra, elemental analysis, and scanning electrical microscopy revealed that AA monomers were grafted onto an SA backbone, and that PVP and GE were present in the hydrogel network as linear interpenetrating components. The grafting polymerization and crosslinking reaction between only SA and AA yielded a bulk gel, but the introduction of PVP and GE into the reaction mixture led to the formation of granular products. Electrostatic and hydrogen-bonding interactions among SA, PAA, PVP, and GE were the main driving forces for the formation of granular products. The adsorption isotherms and adsorption kinetics were evaluated for the adsorption of model heavy-metal ions on one of the hydrogels. The results indicated that the hydrogel has satisfactory adsorption capacities (3.028 mmol/g, Ni^{2+}; 3.146 mmol/g, Cu^{2+}; 2.911 mmol/g, Zn^{2+}; 2.862 mmol/g, Cd^{2+}), adsorption rates, and recovery capacities for the target metal ions. In addition, competitive adsorption results suggested that the hydrogel has a stronger affinity for Cu^{2+} ion than for the other ions.

Keywords Sodium alginate · Granular hydrogel · In situ formation · Adsorption · Heavy metals

W. Wang · Y. Kang · A. Wang (✉)
Center for Eco-material and Green Chemistry, Lanzhou Institute of Chemical Physics, Chinese Academy of Sciences, Lanzhou 730000, People's Republic of China
e-mail: aqwang@licp.cas.cn

Introduction

Hydrogels are polymeric materials (with various functional groups) that show moderate crosslinking into three-dimensional networks, and thus they also present a high degree of flexibility in structural design. By virtue of these advantages, hydrogels play important roles in many fields; for example, they are used in superabsorbent materials [1–4], drug-delivery carriers [5, 6], wastewater decontamination processes [7–9], catalyst carriers [10, 11], smart materials [12], and tissue engineering [13, 14].

Recently, the utilization of hydrogels as adsorbents for the removal of heavy-metal pollutants from water bodies has shown great potential, as most of these pollutants (i.e., Ni^{2+}, Cu^{2+}, Zn^{2+} and Cd^{2+} ions) are increasingly seen as a threat to human health and the environment [15, 16]. Traditional adsorbents (i.e., active carbon, clay, ion-exchange resins) can adsorb such species into pores or onto a large surface area, where hydrogels complex with metal ions through the functional groups (i.e., $-COOH$, $-SO_3^{2-}$, $-C{=}O(NH_2)$, $-SH$, $-COO^-$, $-NH_2$, and $-OH$) in their network structures, and slight swelling of the three-dimensional networks of hydrogels is beneficial to reduce mass-transfer resistance. Hydrogels possess relatively high adsorption capacities and adsorption rates [17, 18]. Many hydrogels intended for use as absorbents were prepared via the polymerization and crosslinking of petroleum-based monomers [19–22], but their disadvantages—they are expensive and are not reusable or biodegradable—have limited their application due to the growing public attention focused on energy sources, resources, and the environment [23, 24]. Hence, the development of novel "green" biopolymer-based hydrogel materials for the twenty-first century [25] has become a subject of great interest.

Sodium alginate (SA) is extracted from marine algae or produced by bacteria. It is also a natural anionic biopolymer that consists of poly-β-1,4-D-mannuronic acid (M units) and α-1,4-L-glucuronic acid (G units), in varying proportions, that are connected by 1–4 linkages. Like other biopolymers, SA is abundant, renewable, nontoxic, water-soluble, biodegradable, and biocompatible. Crosslinked alginate shows excellent adsorption of Pb(II) ions [26], and its adsorption properties can be further enhanced by performing a simple grafting modification [27, 28]. Thus, SA is a promising starting material for developing eco-friendly hydrogel adsorbents with satisfactory adsorption performance.

However, traditional alginate-based hydrogels are bulk gel-like products [8] that require large amounts of energy to dry, smash, and granulate them. In addition, the undesirable homopolymers in the bulk gel are difficult to remove. Thus, much research effort has been expended with the aim of producing a granular hydrogel in a polymerization reaction in order to simplify postprocessing (i.e., oven-drying, smashing, and granulation). Emulsion polymerization or reverse-phase suspension polymerization has usually been adopted for this purpose. Helwa et al. prepared aptamer-functionalized hydrogel microparticles by emulsion polymerization and used them for the fast visual detection of mercury(II) and adenosine [29]. Liu et al. prepared granular superabsorbent hydrogels with nitrogen fertilizers by reverse phase suspension polymerization [30]. Although a granular product was obtained, the reaction process required large amounts of toxic organic solvents and surfactants, was expensive, and was not eco-friendly. Thus, the development of a green polymerization process that yields granular anionic alginate-based hydrogels is a highly attractive goal.

As described previously, the nanoparticles [31] can be prepared in aqueous solution using chitosan and acrylic acid as the raw materials. Electrostatic and hydrogen-bonding interactions are thought be crucial factors in the particle formation process. Based on this, we prepared granular hydrogels via interactions between the cationic polymer chitosan and the anionic polymer poly(acrylic acid) [32], but it proved difficult to form granular anionic biopolymer-based hydrogels using this approach. It was found that the type of positively charged polymer employed is an important influence on the formation of granular products based on anionic biopolymers. Polyvinylpyrrolidone (PVP) is water-soluble linear polymer that is nontoxic, biodegradable, and biocompatible [33], and is frequently used as a dispersant to assist in the preparation of particles [34]. Gelatin (GE) is an ionic and hydrophilic linear polymer with –NH$_2$ and –COOH functional groups. The N moieties of PVP and GE can be protonated, which makes them electropositive and able to act as suitable positively charged components for preparing a granular hydrogel.

Thus, in the work described in the present paper, we successfully prepared granular SA-based hydrogels (SA-g-PAA/PVP/GE) in an aqueous solution by a one-step polymerization reaction, using PVP and GE as an additive and a dispersant. The structures and morphologies of the hydrogels produced in this manner were characterized by Fourier transform infrared spectra (FTIR), elemental analysis (EA), and scanning electrical microscopy (SEM). The adsorption and recovery properties of one of the hydrogels for the adsorption of Ni^{2+}, Cu^{2+}, Zn^{2+} and Cd^{2+} ions were evaluated systematically.

Experimental

Materials

SA, with a kinetic viscosity of 20 cp at 20 °C for a 1 wt% aqueous solution, was purchased from Shanghai Chemical Reagent Co. (Shanghai, China). AA (C.P. grade, Shanghai Shanpu Chemical Factory, Shanghai, China) was distilled under reduced pressure before use. Ammonium persulfate (APS, analytical grade, Xi'an Chemical Reagent Factory, Xi'an, China) and N,N′-methylene-bis-acrylamide (MBA, C.P. grade, Shanghai Chemical Reagent Co.) was used as received. PVP (A.R. grade, relative molecular mass (M_r) 10000, K value 30.0~40.0) was purchased from Tianjin Kermel Chemical Reagents Development Center (Tianjin, China) and used as received. GE (B.C. grade) was purchased from Aladdin Reagent Co. (Shanghai, China) and used as received. Other reagents used were of analytical grade, and all solutions were prepared using distilled water.

Preparation of the granular SA-g-PAA/PVP/GE hydrogel

SA (1 g), GE, and PVP powder (the dosage is listed in Table 1) was dissolved in 50 mL of distilled water at 70 °C in a 250 mL four-neck flask equipped with a reflux condenser, a mechanical stirrer, a funnel, and a nitrogen line. Under stirring, the solution obtained was purged with N$_2$ for 30 min to remove the dissolved oxygen. Then, 10 mL of the aqueous solution of APS (0.015 g) were added and the temperature was kept at 70 °C for 10 min to generate radicals. Subsequently, 15 mL of the aqueous solution containing 7.2 g AA and 0.022 g MBA were added with vigorous stirring. The white granular product appeared after about 10 min. The reaction temperature was kept at 70 °C for 3 h to complete the polymerization. A nitrogen atmosphere was maintained throughout the reaction period.

The granular product was cooled to room temperature and neutralized to pH 7 using 1 mol/L NaOH solution (employing a 2:1 (v/v) methanol/water mixture as the solvent). The neutralized granular gel was immersed in 250 mL of methanol for 24 h to dewater, and this process was repeated four times. Finally, the dewatered granular products were separated by filtration and dried at 60 °C for 2 h to

Table 1 Feed compositions and gel contents (GCs) for the hydrogels, as well as their adsorption capacities for Ni^{2+}, Cu^{2+}, Zn^{2+}, and Cd^{2+} ions

Samples	PVP/GE (m/m)	$m_{\text{(PVP+GE)}}$ (g)	PVP (g)	GE (g)	GC (%)	Adsorption capacities (mmol/g)			
						Ni^{2+}	Cu^{2+}	Zn^{2+}	Cd^{2+}
SA0	–	0	0	0	80.32	2.949	3.087	2.861	2.812
SA1	1.00	1.90	0.95	0.95	94.26	2.954	3.108	2.897	2.845
SA2	1.40	1.90	1.10	0.80	96.40	3.028	3.146	2.911	2.862
SA3	2.10	1.90	1.30	0.60	93.11	2.999	3.058	2.832	2.794
SA4	1.40	1.20	0.70	0.50	93.83	2.911	3.038	2.804	2.755
SA5	1.40	3.50	2.03	1.47	94.52	2.862	3.009	2.795	2.808

a constant weight. The dried product was ground and passed through 80–120 mesh (120~180 μm) for testing. The SA-*g*-PAA hydrogel was prepared by a similar process except without the addition of PVP and GE, and a bulk-form gel was obtained.

Determination of gel content (GC)

Typically, 0.10 g dry sample (m_1) were soaked in 300 mL distilled water for 72 h to extract the soluble constituents. The extracted sample was filtrated and thoroughly oven-dried at 100 °C. The dried samples were weighed (m_2) and the corresponding gel content (%) was calculated using the following equation:

$$\text{GC (\%)} = m_2/m_1 \times 100\%. \tag{1}$$

Adsorption experiments

Adsorption experiments were carried out by bringing 50 mg of the adsorbent into contact with 25 mL of an aqueous solution of Ni^{2+} (9.89 mmol/L), Cu^{2+} (9.92 mmol/L), Zn^{2+} (9.82 mmol/L), or Cd^{2+} (9.93 mmol/L) in a thermostatic shaker (THZ-98A, Chincan, Zhejiang, China) at 30 °C and 120 rpm for 60 min to achieve adsorption equilibrium. The adsorbents were separated from the solution by a sintered glass filter. The filter and adsorbents were washed and all of the solutions were collected together. The solutions created before and obtained after adsorption were diluted to a constant volume, and the amount of metal ion in the solution was measured using an atomic absorption spectrophotometer (AAS, Z-8000, Hitachi, Tokyo, Japan). The data were used to calculate the adsorption capacity of the hydrogel for each metal ion according to the following equation:

$$q = (0.025C_{\text{o}} - V_{\text{e}}C_{\text{e}})/w. \tag{2}$$

Here, q is the amount of metal ion adsorbed at time t (q_t, mmol/g) or at equilibrium (q_e, mmol/g), C_0 is the initial concentration of metal ion (mmol/L), V_eC_e is the number of moles of metal ion in the solution after adsorption (mmol), and w is the mass of adsorbent used (g).

As shown in Table 1, the hydrogel adsorbent SA2 showed the highest adsorption capacity and gel content (96.4 %), and so it was used as the optimal sample to evaluate the adsorption isotherms and kinetics. Typically, a set of Ni^{2+}, Cu^{2+}, Zn^{2+}, and Cd^{2+} solutions at concentrations of 3.06–24.95 mmol/L were used to study the adsorption isotherms, and aqueous solutions containing Ni^{2+} (9.89 mmol/L), Cu^{2+} (9.92 mmol/L), Zn^{2+} (9.82 mmol/L), or Cd^{2+} (9.93 mmol/L) ion were used to evaluate the adsorption kinetics (the adsorption capacity q_t versus the time t).

A mixed solution containing various metal ions at initial concentrations of 2.46 mmol/L (Ni^{2+}), 2.48 mml/L (Cu^{2+}), 2.43 mmol/L (Zn^{2+}), and 2.41 mmol/L (Cd^{2+}) and at an initial pH of 5.0 was used to perform the competitive adsorption experiments. All experiments were carried out in parallel six times, and the averages were used in the analysis.

Evaluation of reusability

In order to evaluate the recovery capacities of the hydrogel adsorbents, different amounts of each hydrogel were brought into full contacted with 25 mL of an aqueous solution of Ni^{2+} (C_1, 9.89 mmol/L), Cu^{2+} (C_1, 9.92 mmol/L), Zn^{2+} (C_1, 9.82 mmol/L), or Cd^{2+} (C_1, 9.93 mmol/L) and allowed to reach adsorption equilibrium. The metal-ion-loaded hydrogel was then soaked in 25 mL of 0.1 mol/L HCl solution and stirred for 60 min to release the metal ions. The adsorbent was separated from the solution by centrifugation and washed with distilled water three times. All of the solutions were then collected together and diluted to a constant volume of 50 mL. Finally, the ion concentration (C_2, mmol/L) in the solution was measured and used to calculate the recovery ratio via

$$\text{Recovery ratio}(\%) = (50C_2/25C_1) \times 100\%. \tag{3}$$

Characterizations

FTIR spectra were recorded on a Nicolet (Vernon Hills, IL, USA) NEXUS FTIR spectrometer in the 4000–400 cm^{-1} region using KBr pellets. Elemental analysis (C, H, and N) was performed using an Elementar (Hanau, Germany) Vario EL elemental analyzer. SEM observations were carried out using an SEM (JSM-5600LV, JEOL, Tokyo, Japan) after coating the sample with a layer of gold film.

Results and discussion

Preparation of granular SA-g-PAA/PVP/GE hydrogels

The granular SA-based hydrogels were formed in aqueous solution through chemical and physical processes such as the grafting of AA onto SA chains, the cross-linking action of MBA, as well as the electrostatic interaction of PVP and GE with the SA and grafted PAA chains (Fig. 1). During the reaction, the initiator APS was decomposed by heating the solution to generate sulfate anion radicals. These radicals stripped the hydrogens from –OH groups on SA chains to form active macroradicals [35] the trigger the vinyl groups of AA to proceed with chain propagation. The PVP and GE were protonated by the H$^+$ of AA and showed electropositivity. This meant that they were able to participate in electrostatic and hydrogen-bonding interactions with the negatively charged SA and grafted PAA chains, thus increasing the entanglement among the polymer chains. Simultaneously, the end vinyl groups of the crosslinker MBA were able to participate in the crosslinking reaction, facilitating the construction of a polymeric network.

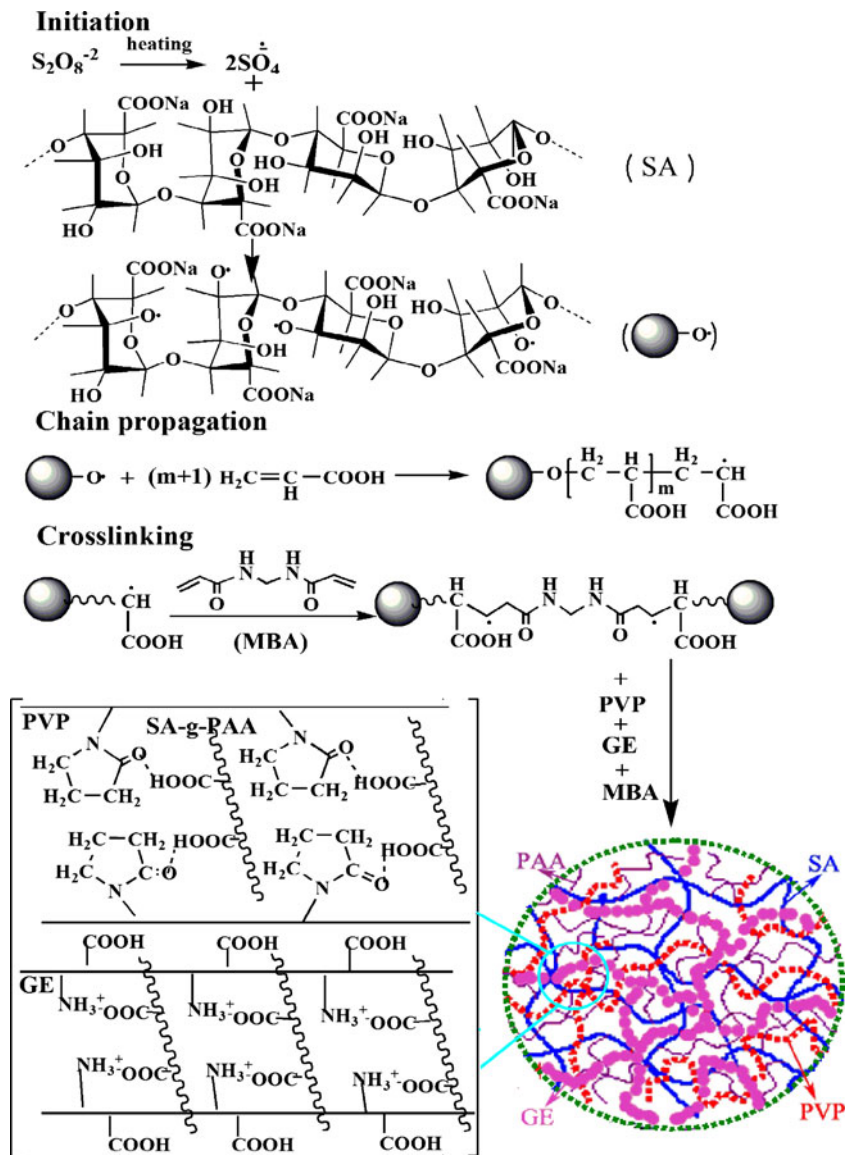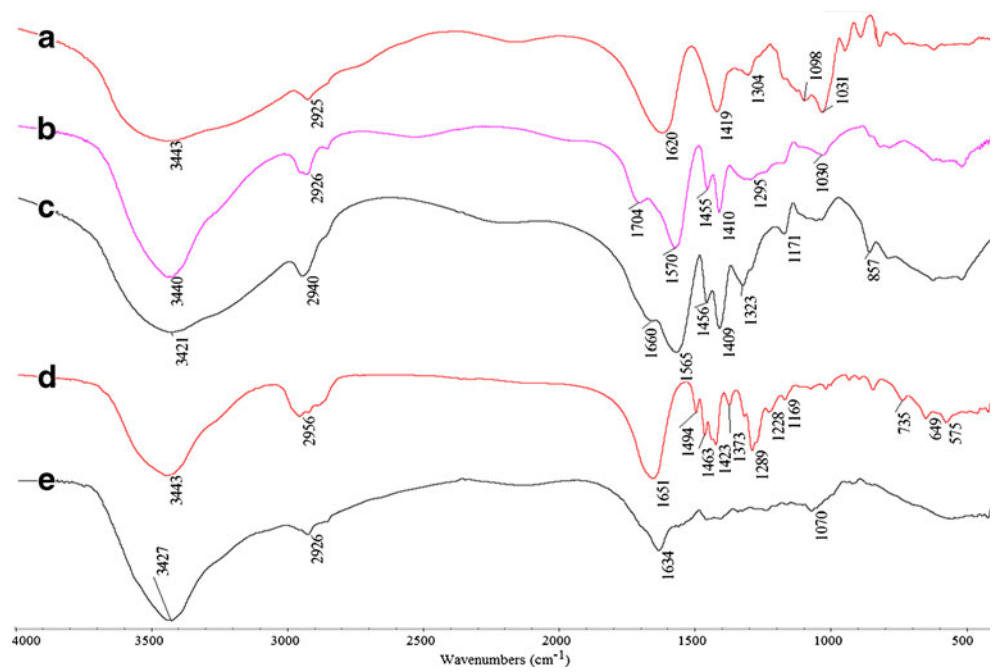Fig. 1 Proposed mechanism for the formation of the hydrogel network

Fig. 2 FTIR spectra of (*a*) SA, (*b*) SA-*g*-PAA, (*c*) SA-*g*-PAA/ PVP/GE (SA2), (*d*) PVP, and (*e*) GE


These interactions prompted the association of AA, SA, PVP, and GE and induced the formation of granular product. In addition, PVP and GE are good dispersants to use in the preparation of nanoparticles, so their dispersive action is favorable to the formation of a stable granular product.

FTIR spectral analysis

FTIR spectra of SA, SA-*g*-PAA, SA-*g*-PAA/PVP/GE (SA2), PVP, and GE are shown in Fig. 2. It can be seen that the characteristic absorption bands of SA at 1098 cm^{-1} and 1031 cm^{-1} (stretching vibrations of C–OH groups) were

Fig. 3 a–e Digital photos of **a** the SA-*g*-PAA hydrogel in the wet state, **b** the SA-*g*-PAA/ PVP/GE (SA2) hydrogel in the wet state, and **c** the SA-*g*-PAA/ PVP/GE (SA2) hydrogel in the dry state. SEM micrographs of **d** SA-*g*-PAA and **e** SA-*g*-PAA/ PVP/GE (SA2) are also shown
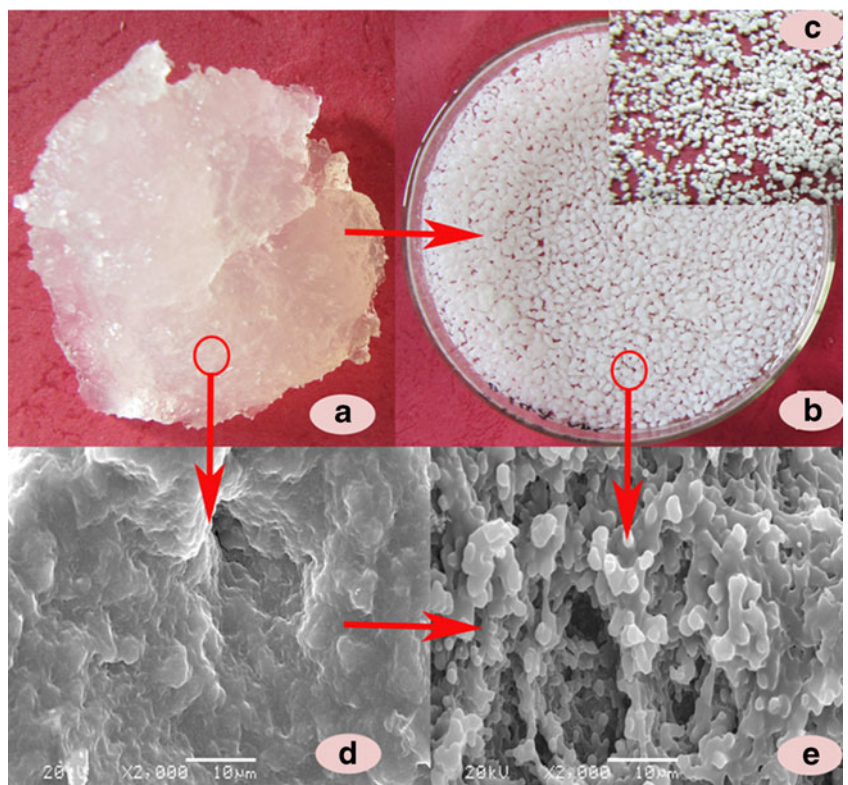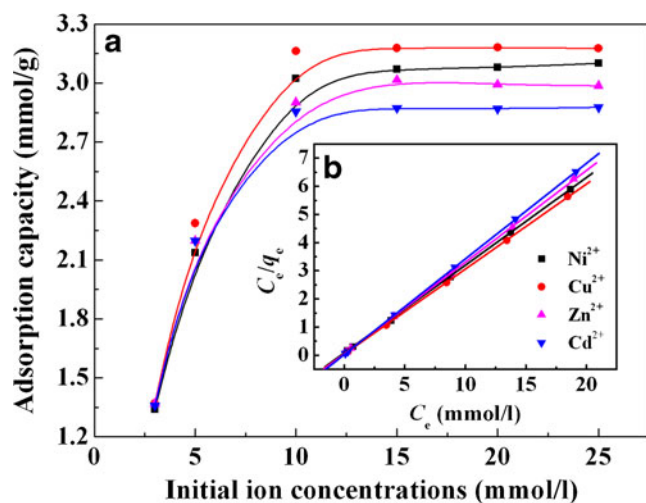
Fig. 4 a–b Effect of initial ion concentration on the adsorption capacity of the granular hydrogel SA2 (a), and plots of C_e/q_e versus C_e for the Langmuir isotherm model (b)

clearly weaker after the reaction (Fig. 2a, b), while new absorption bands appeared at 1704 cm^{-1} (C=O asymmetric stretching vibrations of –COOH groups), 1570 cm^{-1} (C=O asymmetric stretching vibrations of –COO$^-$ groups), 1454 and 1409 cm^{-1} (COO symmetric stretching vibrations of –COO$^-$ groups) in the FTIR spectrum of SA-g-PAA (Fig. 2b). This indicates that AA monomers have been grafted onto the SA chains. The absorption bands of PVP at 1651 cm^{-1} were assigned to the –C=O stretching vibration of PVP, and the band of GE at 1634 cm^{-1} is due to the absorption of –C=O and –NH$_2$ of GE. After the granular hydrogel had formed, the C=O absorption band from –COOH groups at 1704 cm^{-1} (for SA-g-PAA) shifted to 1660 cm^{-1} (for SA2), and the asymmetric stretching vibration of –COO$^-$ groups at 1570 cm^{-1} (for SA-g-PAA) shifted to 1565 cm^{-1} (for SA2). This indicates that the C=O groups of PVP (located at 1651 cm^{-1}) and the –NH$_2$ groups of GE (located at 1634 cm^{-1}) generated hydrogen-bonding interactions with the –COOH groups of SA-g-PAA [36]. In order to further confirm the existence of PVP and GE, the nitrogen content of each hydrogel was determined by elemental analysis. The nitrogen content was close to zero for the SA0 hydrogel, whereas it increased to 1.26 % for SA2 and to 1.92 % for SA5. The above results confirm that the linear PVP and GE

polymer chains were present in the crosslinked hydrogel network, and had physically combined with the SA-g-PAA network [37, 38].

Morphological analysis

Figure 3 shows digital photos of hydrogels with and without PVP and GE in the wet state and dry state, as well as SEM micrographs of the bulk and granular hydrogels. As shown in Fig. 3a, the hydrogel adopts a bulk gel-like form without PVP and GE, whereas the hydrogel with PVP and GE is granular (Fig. 3b), indicating that PVP and GE are essential for the formation of the granular product. The granular shape of the hydrogel makes it easy to dewater it, and this shape is retained without mutual aggregation after dewatering (Fig. 3c). The granular product can be used directly as an adsorbent with no need for any grinding process. The SA-g-PAA bulk hydrogel shows a dense and smooth surface (Fig. 3d), whereas the granular hydrogel shows a coarse surface with gaps, pores, and numerous microparticles (Fig. 3e). These particles are closely stacked and connected with each other to form a granular congeries. In order to evaluate the change in porosity, the BET specific surface areas (S) of the bulk hydrogel (SA-g-PAA) and the granular hydrogel (SA2) were determined. The S value of the bulk hydrogel was 0.009 m^2/g, but it increased to 2.871 m^2/g for the granular hydrogel (SA2), which leads to enhanced penetration of external adsorbate into the hydrogel network of SA2.

Adsorption isotherms

Altering the initial ion concentration can affect the driving force for adsorption and thus affect the adsorption behavior of the hydrogel. As shown in Fig. 4a, the amount of Ni^{2+}, Cu^{2+}, Zn^{2+}, and Cd^{2+} adsorbed by the hydrogel gradually increased with increasing initial ion concentration, due to the increased concentration gradient. We utilized three isotherm equations to evaluate the adsorption process and reveal the adsorption mechanism—the models of Langmuir (Eq. 4) [39], Freundlich (Eq. 5) [40], and Dubinin–Radushkevich (D–R) (Eq. 6) [41]:

$$C_e/q_e = 1/(q_m b) + C_e/q_m \tag{4}$$

Table 2 Estimated adsorption isotherm parameters for the adsorption of Ni^{2+}, Cu^{2+}, Zn^{2+}, and Cd^{2+} ions on the hydrogels

Ions	Langmuir equation			Freundlich equation			D–R equation		
	q_e (mmol/g)	b (L/mmol)	R^2	K	n	R^2	q_m (mmol/g)	β (mol^2/kJ^2)	R^2
Ni^{2+}	3.158	3.1455	0.9999	1.9796	5.3127	0.9187	4.3597	0.00254	0.9461
Cu^{2+}	3.221	5.2692	0.9999	2.1670	6.0525	0.8796	4.3025	0.00219	0.9055
Zn^{2+}	3.035	4.5877	0.9999	2.0326	6.1136	0.9125	4.0190	0.00217	0.9397
Cd^{2+}	2.913	5.0144	0.9999	1.9962	6.4851	0.8915	3.8102	0.00206	0.9203

Fig. 5 **a** FTIR spectra of the granular hydrogel before adsorption (*a*) and after adsorbing Ni^{2+} (*b*), Cu^{2+} (*c*), Zn^{2+} (*d*), and Cd^{2+} (*e*); **b** the main mechanism for the adsorption of Ni^{2+}, Cu^{2+}, Zn^{2+}, and Cd^{2+} ions onto the hydrogel
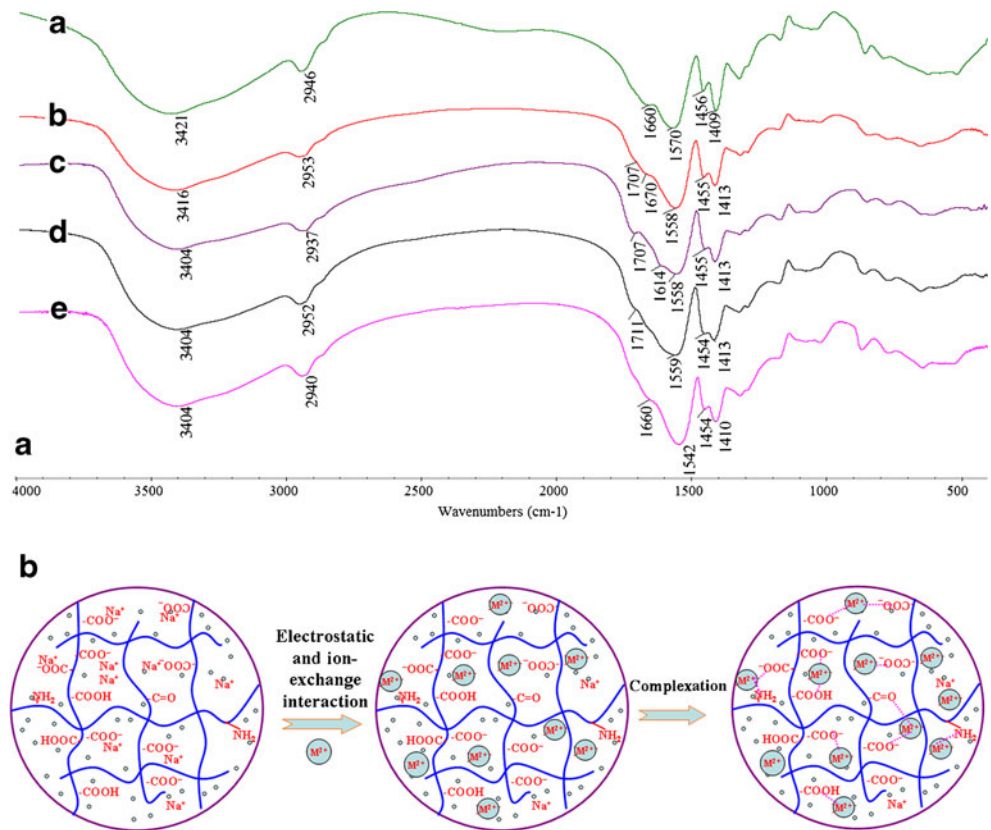
$$\log q_e = \log K + (1/n)\log C_e \qquad (5)$$

$$\ln q_e = \ln q_m - \beta \varepsilon^2. \qquad (6)$$

Here, q_e is the equilibrium adsorption capacity (mmol/g), C_e is the concentration of metal ion after adsorption (mmol/L), q_m is the maximum adsorption capacity (mmol/g), and b is the Langmuir adsorption constant (L/mmol), which is
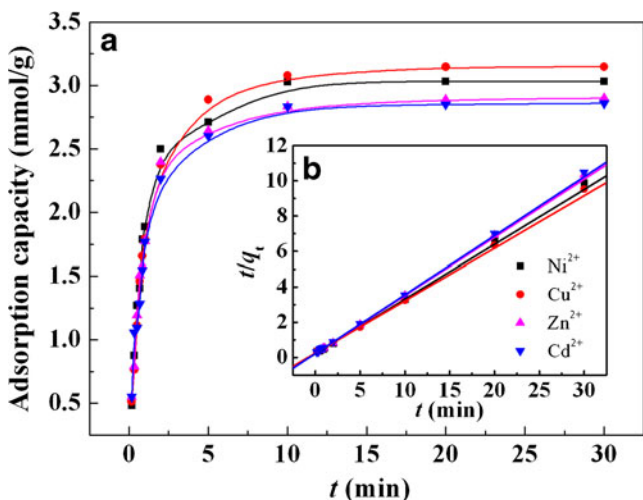

Fig. 6 a Adsorption kinetic curves for the adsorption of metal ions onto the granular hydrogel, and **b** plots of t/q_t versus t

related to the free energy of adsorption. K (L/g) and n (dimensionless) are the Freundlich isotherm constant and the heterogeneity factor, respectively. β is a constant related to the mean free energy of adsorption ($mol^2 \ kJ^{-2}$). ε is the Polanyi potential and is equal to $RT\ln(1+(1/C_e))$, where R (8.314 J/(mol K)) is the gas constant and T (K) is the absolute temperature. These parameters can be obtained by fitting the Langmuir (plotting C_e/q_e vs C_e), Freundlich (plotting $\log q_e$ vs $\log C_e$), and D–R (plotting $\ln q_e$ vs ε^2) equations to the adsorption data (Table 2). As can be seen, when the Freundlich isotherm model ($R^2 < 0.9187$) and the D–R model ($R^2 < 0.9461$) are fitted to the data, there are obvious deviations from the experimental values, whereas the Langmuir isotherm model fits very well to the data ($R^2 = 0.9999$), and the plots of C_e/q_e vs C_e show perfect straight lines (Fig. 4b). This indicates that the Langmuir model is suitable for describing the adsorption isotherm. Generally, Langmuir's model of adsorption (Eq. 3) predicts the existence of a monolayer of the adsorbate on the outer surface of the adsorbent. The Freundlich isotherm model (Eq. 4) describes reversible adsorption, and is not restricted to the formation of a monolayer. Therefore, we can conclude that a monolayer of Ni^{2+}, Cu^{2+}, Zn^{2+}, or Cd^{2+} ion was formed on the surface of the hydrogel.

In this study, the granular hydrogel used had an interconnected three-dimensional network and equally distributed $-COO^-$, $-COOH$ and $-NH_2$ functional groups. The metal

Table 3 Estimated adsorption kinetic parameters for the adsorption of Ni^{2+}, Cu^{2+}, Zn^{2+}, and Cd^{2+} on the hydrogel

	Pseudo-first-order model				Pseudo-second-order model			
	q_e (exp) mmol/g	q_e (cal) mmol/g	k_1 min^{-1}	R^2	q_e (cal) mmol/g	k_2 g/(mmol min)	k_{2i} mmol/(g min)	R^2
Ni^{2+}	3.028	2.0908	0.4687	0.9879	3.123	0.4603	4.4895	0.9998
Cu^{2+}	3.146	2.2052	0.3749	0.9966	3.255	0.3740	3.9621	0.9999
Zn^{2+}	2.911	2.2088	0.3994	0.9635	2.998	0.5074	4.5602	1
Cd^{2+}	2.862	1.5390	0.2874	0.9585	2.940	0.4985	4.3087	0.9999

ions can penetrate into the 3D polymeric network due to electrostatic attractions between negatively charged –COO$^-$ groups and the cationic metal ions as well as ion exchange between Na$^+$ ions in the network and external metal ions. After entering the network, the heavy-metal ions chelate with the functional groups, and a chemical adsorption process occurs. In order to confirm this, FTIR spectra were obtained for the granular hydrogel after it had adsorbed Ni^{2+}, Cu^{2+}, Zn^{2+}, and Cd^{2+} ions (Fig. 5a). We found that the asymmetric stretching vibrations of –COO$^-$ groups at 1570 cm^{-1} before adsorption shifted to 1558, 1558, and 1559, or 1542 cm^{-1} upon the adsorption of Ni^{2+}, Cu^{2+}, Zn^{2+}, or Cd^{2+} ions, respectively, indicating that the –COO$^-$ groups were complexed with the metal ions [18]. The complexation interaction is the main driving force for adsorption, and represents the chemical adsorption mechanism (Fig. 5b).

Adsorption kinetics

As shown in Fig. 6a, the adsorption equilibrium for the adsorption of Ni^{2+}, Cu^{2+}, Zn^{2+}, and Cd^{2+} ions onto the granular hydrogel was achieved within about 5 min. This fast adsorption rate can be ascribed to the following reasons: the granular hydrogel is hydrophilic, and the 3D gel network may expand slightly upon contact with water due to the ionization of the PAA chains and electrostatic repulsion among the polymer chains. As a

result, resistance to the diffusion of the adsorbate decreases, enhancing the adsorption rate. The following pseudo-first-order (Eq. 7) and pseudo-second-order (Eq. 8) kinetic models were used to explore the mechanism controlling adsorption processes such as mass transfer and the chemical reaction [42]:

$$\log(q_e - q_t) = \log q_e - (k_1/2.303)t \tag{7}$$

$$t/q_t = 1/k_2 q_e^2 + t/q_e, \tag{8}$$

where q_e and q_t are the adsorption capacities of the hydrogels at equilibrium and at time t (s), respectively. k_1 and k_2 are the rate constants of pseudo-first-order (min^{-1}) and pseudo-second-order (mmol/g/s) adsorption kinetics. The slope and intercept of the straight lines of $\log(q_e-q_t)$ versus t and t/q_t versus t, respectively, can be used to calculate the rate constants k_1 and k_2 and the initial rate constant k_{2i} (= $k_2 q_e^2$); see Table 3. It was found that the theoretical q_e values obtained from the pseudo-first-order kinetic model did not agree well with the experimental values, whereas the pseudo-second-order kinetic model for the adsorption of metal ions on the hydrogel gave perfect straight lines (Fig. 6b) and better correlation coefficients ($R^2 > 0.9998$). This indicates that the pseudo-second-order kinetic model more accurately reflects the adsorption kinetics than the pseudo-first-order kinetic model does, and the process of adsorption of Ni^{2+}, Cu^{2+},
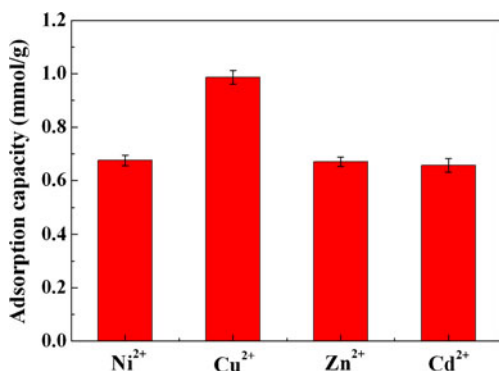
Fig. 7 Competitive adsorption capacities of the hydrogel for Ni^{2+}, Zn^{2+}, and Cd^{2+} ions (the initial ion concentrations were 2.46 mmol/L for Ni^{2+}, 2.48 mml/L for Cu^{2+}, 2.43 mmol/L for Zn^{2+}, and 2.41 mmol/L for Cd^{2+}
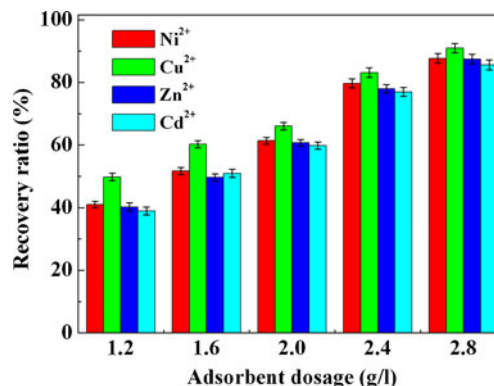
Fig. 8 Recovery capacities of the granular hydrogel SA2 for Ni^{2+}, Cu^{2+}, Zn^{2+}, and Cd^{2+} ions at different dosages

Zn^{2+}, and Cd^{2+} ions onto the granular hydrogel is probably controlled by the chemical adsorption process. According to the calculated kinetic constants (k_{2i}), it was concluded that the initial adsorption rates of the ions onto the hydrogel follow the order $Zn^{2+}> Ni^{2+}> Cd^{2+}> Cu^{2+}$.

Competitive adsorption capability

The existence of multiple ionic species in the solution may affect the adsorption capacity of hydrogel for each ion species. In this section, the competitive adsorption behavior of Ni^{2+}, Cu^{2+}, Zn^{2+}, and Cd^{2+} ions on the SA2 hydrogel was evaluated using a solution containing a mixture of various metal ions (2.46 mmol/L for Ni^{2+}, 2.48 mml/L for Cu^{2+}, 2.43 mmol/L for Zn^{2+}, and 2.41 mmol/L for Cd^{2+}); see Fig. 7. As can be seen, the adsorption capacity of the hydrogel for Cu^{2+} ion (0.987 mmol/g) is clearly higher than that for Ni^{2+} (0.675 mmol/g), Zn^{2+} (0.670 mmol/g), or Cd^{2+} (0.656 mmol/g). This indicates that, among the ions studied, the hydrogel has the strongest affinity for Cu^{2+} ion.

Recovery capacity for heavy-metal ions

For the adsorbent to be practically useful, it allow the simultaneous removal and recovery of heavy metals from aqueous solutions for reuse. Figure 8 shows the recovery capabilities of the granular hydrogel for different concentrations of Ni^{2+}, Cu^{2+}, Zn^{2+}, and Cd^{2+} ions. The recovery ratios increased as the dosage of the hydrogel increased. When the dosage was 2.8 g/L, the recovery ratios reached 87.70 % (Ni^{2+}), 90.92 % (Cu^{2+}), 87.47 % (Zn^{2+}), and 85.55 % (Cd^{2+}), indicating that the hydrogel has excellent recovery capabilities towards heavy-metal ions. The metal ions can be desorbed by applying dilute HCl solution and recovered as a chloride. As discussed above, this eco-friendly granular adsorbent has the potential to be developed into an efficient adsorbent for the simultaneous removal and recovery of metal ions.

Conclusions

The first successful preparation of a granular anionic alginate-based hydrogel was achieved through one-step in situ polymerization in an aqueous solution using SA as the matrix, AA as the monomer, MBA as the crosslinker, and PVP and GE as the interpenetrating components and dispersants. The hydrogel without PVP and GE is a bulk-form gel, whereas the introduction of PVP and GE results in the formation of a granular product. The presence of PVP and GE is therefore essential to the formation of a granular product, and the electrostatic and hydrogen-bonding interactions among PVP, GE, SA, and PAA are the main driving forces for the formation of the granular product. The granular product can be easily dewatered and dried, and can be used directly as an adsorbent with no need for smashing and granulation. The as-prepared granular hydrogel shows enhanced adsorption capacities for divalent heavy metal ions (3.028, 3.146, 2.911, and 2.862 mmol/g for Ni^{2+}, Cu^{2+}, Zn^{2+}, and Cd^{2+}, respectively) and improved adsorption rates. In addition, the hydrogel exhibits satisfactory recovery capabilities for metal ions (87.70 % for Ni^{2+}, 90.92 % for Cu^{2+}, 87.47 % for Zn^{2+}, and 85.55 % for Cd^{2+}), making it a favorable material for facilitating the reuse of valuable metals. Therefore, the one-step-prepared granular hydrogel has various advantages over traditional bulk-form hydrogels in terms of preparation method, saving energy, performance, and the environment, and can be used directly used as an efficient and eco-friendly adsorbent for the removal and recovery of heavy metals from aqueous solution.

References

1. Nakason C, Wohmang T, Kaesaman A, Kiatkamjornwong S (2010) Carbohydr Polym 81:348–357
2. Marandi GB, Mahdavinia GR, Ghafary S (2011) J Polym Res 18:1487–1499
3. Al E, Güçlü G, İyim TB, Emik S, Özgümüş S (2008) J Appl Polym Sci 109:16–22
4. Wang WB, Wang AQ (2010) Carbohydr Polym 82:83–91
5. Kevadiya BD, Joshi GV, Mody HM, Bajaj HC (2011) Appl Clay Sci 52:364–367
6. Ngadaonye JI, Cloonan MO, Geever LM, Higginbotham CL (2011) J Polym Res 18:2307–2324
7. Güçlü G, Al E, Emik S, İyim TB, Özgümüş S, Özyürek M (2009) Polym Bull 65:333–346
8. Guilherme MR, Reis AV, Paulino AT, Fajardo AR, Muniz EC, Tambourgi EB (2007) J Appl Polym Sci 105:2903–2909
9. Milosavljević NB, Ristić MĐ, Perić-Grujić AA, Filipović JM, Štrbac SB, Rakočević ZLJ, Krušić MTK (2011) Colloids Surf A 388:59–69
10. Kangwansupamonkon W, Jitbunpot W, Kiatkamjornwong S (2010) Polym Deg Stab 95:1894–1902
11. Léger B, Menuel S, Ponchel A, Hapiot F, Monflier E (2012) Adv Synth Catal 354:1269–1272
12. Saikia AK, Mandal UK, Aggarwal S (2012) J Polym Res 19:9871
13. Román J, Cabañas MV, Peña J, Vallet-Regí M (2011) Sci Technol Adv Mater 12:045003
14. Zhu JM (2010) Biomaterials 31:4639–4656
15. Sud D, Mahajan G, Kaur MP (2008) Bioresource Technol 99:6017–6027
16. Demirbas A (2008) J Hazard Mater 157:220–229
17. Liu Y, Wang WB, Wang AQ (2010) Desalination 259:258–264
18. Zheng YA, Hua SB, Wang AQ (2010) Desalination 263:170–175

19. Şolpan D, Duran S, Saraydin D, Güven O (2003) Rad Phys Chem 66:117–127
20. Chen H, Wang AQ (2009) J Hazard Mater 165:223–231
21. Pekel N, Güven O (2003) Colloids Surf A 212:155–161
22. Çaykara T, İnam R (2003) J Appl Polym Sci 89:2013–2018
23. Song F, Tang DL, Wang XL, Wang YZ (2011) Biomacromoles 12:3369–3380
24. Avérous L, Pollet E (2012) Biodegradable polymers. In: Environmental silicate nano-biocomposites. Springer, London, pp 13–39
25. Ray SS, Bousmina M (2005) Prog Mater Sci 50:962–1079
26. Stewart TJ, Yau JH, Allen MM, Brabander DJ, Flynn NT (2009) Colloid Polym Sci 287:1033–1040
27. Sand A, Yadav M, Mishra DK, Behari K (2010) Carbohydr Polym 80:1147–1154
28. Yadav M, Mishra DK, Sand A, Behari K (2011) Carbohydr Polym 84:83–89
29. Helwa Y, Dave N, Froidevaux R, Samadi A, Liu JW (2012) ACS Appl Mater Interf 4:2228–2233
30. Liu MZ, Liang R, Zhan FL, Liu Z, Niu AZ (2007) Polym Int 56:729–737
31. Hua Y, Jiang XQ, Ding Y, Ge HX, Yuan YY, Yang CZ (2002) Biomaterials 23:3193–3201
32. Xie YT, Wang AQ (2009) J Polym Res 16:143–150
33. Robinson BV, Sullivan FM, Borzelleca JF, Schwartz SL (1990) PVP: a critical review of the kinetics and toxicology of polyvinyl-pyrrolidone (Povidone), 1st edn. Lewis, Chelsea
34. Hu YG, Zhao T, Zhu PL, Sun R (2012) Colloid Polym Sci 290:401–409
35. Pourjavadi A, Farhadpour B, Seidi F (2008) Starch-Starke 60:457–466
36. Jin SP, Liu MZ, Zhang F, Chen SL, Niu AZ (2006) Polymer 47:1526–1532
37. Žugić D, Spasojević P, Petrović Z, Djonlagić J (2009) J Appl Polym Sci 113:1593–1603
38. Jaiswal M, Koul V, Dinda AK, Mohanty S, Jain KG (2011) J Biomed Mater Res B 98B:342–350
39. Langmuir I (1918) J Am Chem Soc 40:1361–1403
40. Freundlich HMF (1906) Z Phys Chem 57:385–470
41. Dubinin MM, Radushkevich LV (1947) Equation of the characteristic curve of activated charcoal. Proc Acad Sci USSR 55:331–333
42. Rudzinsk W, Plazinski W (2006) J Phys Chem B 110:16514–16525